Multi-wavelength Calibration Procedure for the Pierre Auger Observatory Fluorescence Detectors

A.C. Rovero[*,a,1], P. Bauleo[b], J.T. Brack[b], J.L. Harton[b], and R. Knapik[b], for the Pierre Auger Collaboration

[a] *Instituto de Astronomía y Física del Espacio (CONICET), CC 67 Suc 28 (C1428ZAA) Buenos Aires, Argentina*
[b] *Colorado State University, Department of Physics, Fort Collins CO 80523, USA*

Abstract

We present a method to measure the relative spectral response of the Pierre Auger Observatory Fluorescence Detector. The calibration was done at wavelengths of 320, 337, 355, 380 and 405 nm using an end-to-end technique in which the response of all detector components are combined in a single measurement. A xenon flasher and notch–filters were used as the light source for the calibration device. The overall uncertainty is 5%.

Key words: Auger Observatory, Extensive Air Shower, Fluorescence detectors, calibration, cosmic ray
PACS: 95.55.Cs, 96.50.sd

[*]Corresponding author. e-mail: rovero@iafe.uba.ar
[1]Member of Carrera del Investigador, CONICET

1. Introduction

The Pierre Auger Observatory has been designed to measure Extensive Air Showers (EAS) initiated by cosmic rays with energies above 10^{18} eV. The Observatory calls for the construction of two large detectors, one in the southern hemisphere and one in the northern hemisphere, each covering an area of at least 3000 km^2 [1]. The Southern Observatory original baseline design in Malargüe, Argentina, is completed and consists of two detectors, the Surface Detector (SD) and the Fluorescence Detector (FD). The SD is composed of 1600 water Cherenkov detectors located on a triangular array of 1.5 km spacing to measure the EAS secondary particles reaching ground level. In addition, the UV-nitrogen fluorescence light produced in air is registered by the FD during dark, clear nights. The FD consists of 24 telescopes distributed in four buildings, or FD stations, overlooking the SD array.

The energy calibration of data taken at the Pierre Auger Observatory relies on the calibration of the FD [2] [3]. A detailed description of the fluorescence detector can be found elsewhere [4]. The Auger FD telescopes use Schmidt optics. The aperture is defined by a 2.2 m optical diaphragm. A UV filter covers the aperture and reduces background light by cutting out all light not in the main part of the nitrogen fluorescence spectrum ($\sim$300 - 400 nm). It also provides ambient isolation, which allows for temperature controlled operation of the telescope and prevents dust from entering the optical system. Spherical aberrations are reduced by a Schmidt corrector annulus covering only the outer portion of the aperture. Light is concentrated by a 3.5 m $\times$ 3.5 m tessellated spherical mirror into an array of 440 hexagonal photomultipliers (PMTs), referred to as "pixels", with a field of view of 1.5 deg each. At the focal plane, light concentrators approximating hexagonal Winston cones reduce dead spaces between PMTs. The pixel array is referred to as a "camera". In Fig. 1 we show the main components of the FD telescope.

To calibrate the FD three different procedures are performed [5]: the relative, the absolute and the multi-wavelength calibrations. Relative calibration is performed at least at the beginning and at the end of every observing night. It is based on uncalibrated but stable light sources that illuminate the camera from three positions upstream in the optical system, tracking the nightly response variations of the whole system [6]. The absolute calibration is made by an end-to-end technique, using a calibrated portable light source in front of the telescope aperture, which calibrates the combined effect of each component in a single measurement at a single wavelength, 375 nm.

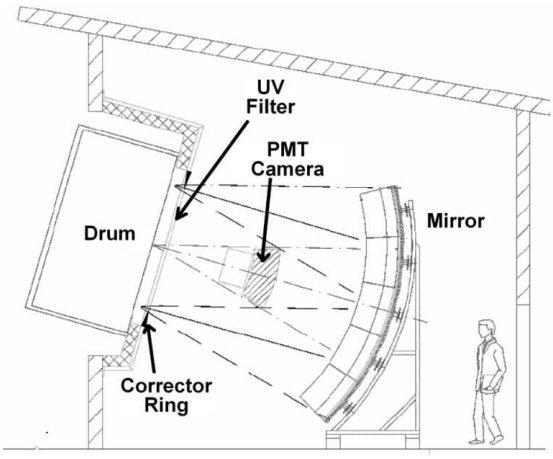

Figure 1: Sketch of the fluorescence detector showing its main components, together with the calibration light source (drum) in calibration position. PMT camera supports and drum supports are not shown for clarity.

The light source has been designed to uniformly illuminate all 440 pixels in a single camera simultaneously and is referred to as the "drum" because of its appearance. It is a cylinder of 2.5 m diameter and 1.4 m deep, with one Teflon® face, and internally laminated with Tyvek® (see Fig. 2). When used for absolute calibration of FD telescopes, a UV LED is placed inside a small Teflon diffuser inside the drum, and surrounded by other diffusive pieces in such a way that the face is uniformly illuminated. The procedure to calibrate the drum at the laboratory has been outlined elsewhere for the prototype [7] and for the current version of the drum [8]. Absolute calibration of FD telescopes is performed typically twice a year to follow long term variations of the system response. Finally, a "multi-wavelength calibration" procedure determines the spectral response of the system as a function of photon wavelength. This is a relative measurement, normalised to the absolute calibration at 375 nm. The multi–wavelength calibration is needed not only for correct event reconstruction but also to correlate with the results of alternative absolute calibrations performed at different wavelengths using lasers. Changes in the spectral response of the FD are not expected to occur in the short term, thus the frequency for evaluating this dependence is planned to be less than once per year.

In this work, we describe the procedure for multi-wavelength calibration of

fluorescence telescopes using an end-to-end technique similar to that used for the absolute calibration. We describe the initial spectral dependence function used by the Auger Observatory in section 2. The new light source used in the procedure is described in section 3 and its characterisation in section 4. The FD-telescope wavelength response and a discussion of uncertainties are presented in section 5.

2. Piecewise spectral response of the fluorescence detector

The spectral response of the FD originally used by the Auger Observatory was assembled from the efficiencies of the individual telescope components. The individual efficiencies were obtained from statements by the component manufacturers or, in some cases, as measured by members of the Pierre Auger Collaboration [9]. The elements considered for the spectral response were the UV filter and corrector ring transmission, the mirror reflectivity, and the PMT quantum efficiency. The overall wavelength response is dominated by filter and PMT effects. We call this piece-wise curve $PW(\lambda)$ and show it in section 5 to compare it with results in Fig. 7.

Regardless of the accuracy of the measurements on each telescope component, the fact that the response of the system was not measured as a whole indeed introduces uncertainties. We can calculate, for example, that the corrector ring transmission does not affect all the incoming photons but only approximately half of them, when camera shadowing effects are included. Also, the reflectivity of the light concentrators in the camera are not taken into account at all, even though a third of the light getting to the pixel is reflected by them. There are other less important considerations such as the fact that mirrors for the FD telescopes are made using two different techniques by two different manufacturers [10]. One of them is a machined aluminium alloy with a protecting layer of Al_2O_3 at its reflecting surface. In the second technique polished glass is aluminized and the reflecting surface is covered by a layer of SiO_2. Both types of mirrors have similar reflectivities as measured at 370 nm [10]. However, considering that they use different dielectric coatings on different materials, the reflectivity at other wavelengths may vary.

To assure that the Pierre Auger Observatory is using the right spectral response of its FD telescopes, the decision was made to adapt the end-to-end procedure used for absolute calibration to directly measure this function.

3. Multi-wavelength light source

To enable multiple wavelength measurements, the LED used for absolute calibration was removed and a light pipe was installed between the Teflon diffuser and the back of the drum, where new light sources could be mounted (see Fig. 2). A xenon flasher is mounted at the end of the pipe at the back of the drum. The xenon flasher[2] provides 0.4 mJ optical output per pulse covering a broad UV spectrum, in a time period of a few hundred nanoseconds. To select a desired wavelength, notch-filters[3] are mounted in a filter wheel attached to the end of the pipe. A focusing lens at the filter wheel output maximises the intensity through the filter wheel and into the light pipe. Notch-filters were chosen at five wavelengths inside the range of the FD UV filter located at the telescope aperture. According to the manufacturer, the filter transmissions are centred at 320, 337, 355, 380 and 405 nm, with a FWHM $\approx$ 15 nm.

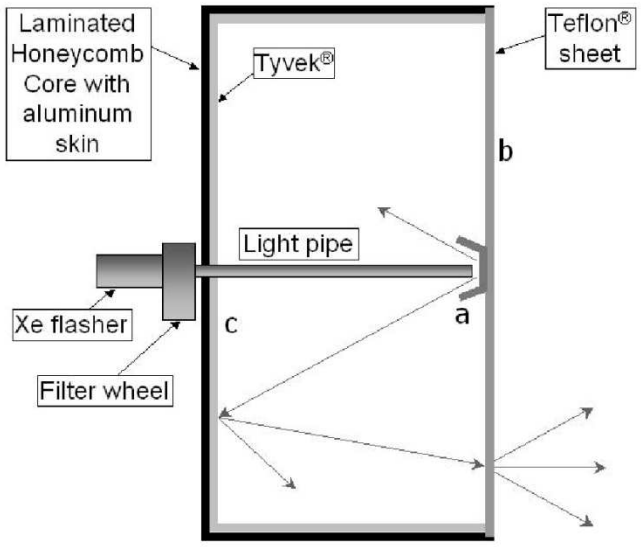

Figure 2: Drum section showing the main components of the light source. The diffusively reflecting surfaces a) and b) are Teflon, while c) is Tyvek

[2]RSL-2100 series xenon flasher - Perkin Elmer, www.perkinelmer.com
[3]Standard UV bandpass filters, Andover Corporation, www.andcorp.com

4. Characterization Measurements

The drum relative intensity is measured at each wavelength in a dedicated calibration laboratory at the Observatory. An auxiliar PMT, the "lab-PMT", is used to measure the light intensity of the drum for a given notch-filter. Quantum efficiency (QE) of the lab-PMT and FD spectral response have significant variations within the range of wavelengths where the notch-filters transmit. To understand the corrections to be applied due to these variations we have performed measurements described in the following sections.

4.1. Notch-filter transmission scan

Notch-filters listed in section 3 were selected at 5 wavelengths either near the main emission bands of nitrogen [11] used for EAS fluorescence detection (320, 355 and 405 nm), or to match the laser wavelengths (337 and 355 nm) used in previous absolute calibration cross checks using roving lasers [5], or near the 375 nm LED single–wavelength absolute calibration. Precise measurements of the transmission characteristics of each notch-filter are needed. The filters were scanned using a monochromator with a broadband deuterium light source. A photo-diode of known wavelength dependence [12] was used at the monochromator output to detect the transmitted light as a function of wavelength in 2 nm steps. The results are shown in Fig. 3 where the spectral shape of the deuterium light source and the response of the photo-diode have been deconvolved. We assign labels of $f_i(\lambda)$ to the curves in the figure and λ_i to the central wavelength of each of them, where $i = 1, 5$ indicates one of the five notch-filters (from 320 nm to 405 nm). A scan from the manufacturer was available for one of the filters (337 nm), and it was found to be in good agreement with our scan. Some asymmetries were found in the transmission curves (320 and 337 nm) that make significant differences when applying filter corrections.

4.2. Quantum efficiency of the lab-PMT

We measured the relative quantum efficiency of the lab-PMT in 2 nm steps using the deuterium light source and the monochromator. We directed the monochromator output through a thin Teflon diffusor and into a dark box containing the lab-PMT and a NIST-calibrated photo-diode[4] [12]. Using the small photo-diode we verified that the beam was uniform laterally at a

[4]UV100 photodiode, UDT Sensors, Inc, Hawhorne, CA USA

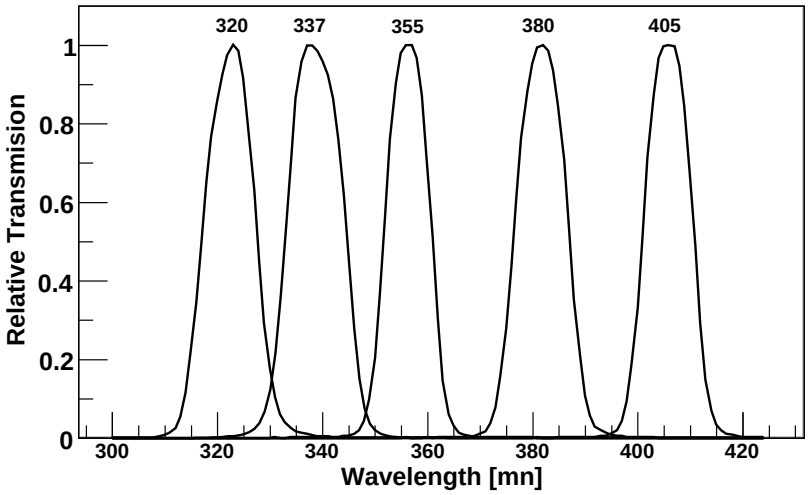

Figure 3: Relative transmission of the notch-filters used for multi-wavelength calibration. The nominal wavelength is indicated for each filter

level of 0.5% over an area larger than the PMT photochathode. The first step in the QE measurement was to scan the monochromator and measure the relative output intensity in photons at each wavelength, using the photodiode and it's known calibration. Then, using an iris to limit the intensity and prevent PMT saturation, we rescanned the source and measured the PMT current. The PMT relative QE as a function of wavelength, $QE(\lambda)$, is the ratio of these two scan results at each wavelength.

The measured QE, shown in Fig. 4, is in agreement with the average photocathode QE provided by the manufacturer[5], within the measurement uncertatities of 2.5%, which are discussed in section 5.2.

4.3. Drum Intensity at five wavelengths

With the notch-filter wheel mounted on the drum, the relative intensity of the drum surface for each wheel position depends on the xenon source intensity at the transmitted wavelengths, the notch-filter transmission and losses in the light pipe. No wavelength shifting of photons of Teflon and Tyvek

[5]78 mm, 9265B PMT, made by Electron Tubes, www.electrontubes.com

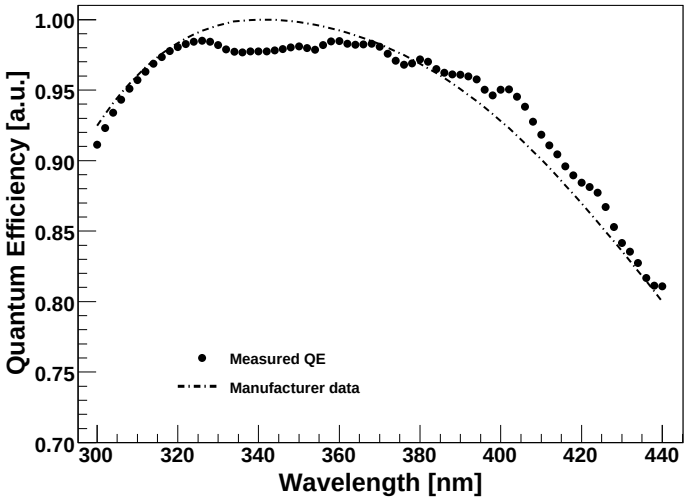

Figure 4: The measured quantum efficiency of the lab-PMT used in this work, and the typical QE from the manufacturer's specification sheet

materials has been observed in our independent laboratory measurements. Ideally, to measure the drum intensity for each wavelength, one would use the drum surface as input to the monochromator and scan the full spectrum for each notch-filter. In practice this is precluded by the low drum intensity. Instead, we make a single measurement of the integrated drum intensity for each notch-filter using the lab-PMT. For each notch-filter we find a value for C_i, the centroid of the histogram of the PMT response to 1000 xenon flasher pulses. These centroids are proportional to the drum intensity for each notch-filter once corrections have been made for variations in lab-PMT QE. Ignoring common constants, $\int \Phi_i(\lambda)\ QE(\lambda)\ d\lambda = C_i$, where $\Phi_i(\lambda)$ is the brightness of the drum surface for the notch-filter i as a function of wavelength. Then, since the distribution of drum photons is the convolution of the known xenon flasher spectrum, $Xe(\lambda)$, and the corresponding notch-filter, we use $\Phi_i(\lambda) = k_i f_i(\lambda)\ Xe(\lambda)$ and adjust k_i to match the integral above. With this last process all five values of drum brightness and their wavelength distributions are known.

The quantity $\int \Phi_i(\lambda)\ d\lambda = \Phi_i$ is proportional to the real total photon flux being emitted by the drum surface. All the wavelength independent properties (PMT gain, electronic conversion, etc.) are left out because they will

cancel in the end when the relative values are computed. We also note that Φ_i is not significantly different from the value it would have if the function $QE(\lambda)$ was totally flat within the notch-filter range. Then, in practice,

$$\int \Phi_i(\lambda)\, d\lambda = \Phi_i \simeq C_i/QE(\lambda_i) \tag{1}$$

5. Fluorescence Detector response to drum

For testing the procedure we use results of measurements made at one FD telescope. In August 2006 we mounted the drum with xenon flasher and filter wheel at the aperture of telescope 4 at the Los Leones FD–building. A series of 400 xenon flashes illuminated the camera, and we found the average integrated pulse for each pixel. In Fig. 5 we show the response of one FD pixel and the distribution of pulse integrals for the same pixel. The pulse shape from the drum with the xenon source is irregular and varies from pulse to pulse, but the total output energy is consistent as indicated by the <10 % RMS of the integral distributions. We obtained the average charge from the distributions of those 400 pulse integrals, $I_{i,j}$, for each notch-filter i and each pixel j. Typical statistical uncertainty for these values is <0.5 %.

The relative wavelength-dependent FD response for pixel j is then the ratio of the integrated ADC response of the FD to the relative number of photons at the aperture. We call this value $R_{i,j}$ so that $R_{i,j} = I_{i,j}/\Phi_i$. A considerable dispersion of $R_{i,j}$ values is expected as pixels have different gains and amplifications. However, we are only interested in relative wavelength responses so, all values are normalized to the response to the 380 nm notch-filter, or $i = 4$. Thus $R^{rel}_{i,j} = R_{i,j}/R_{4,j}$. In Fig. 6 the distribution of these relative responses for pixels in the measured telescope is shown for each notch-filter, except the one at 380 nm as this would be the identity. The histograms shown for each notch-filter in Fig. 6 have relatively low dispersions, ranging from 1.1% to 2.2% RMS. We consider that the relative response for each PMT in the camera is well represented by the average of those distributions, so only one value for each notch-filter is taken. We call these values R^{rel}_i, where i identifies the filter.

In Table 1 we show the R^{rel}_i values obtained for the telescope as evaluated from the distributions on Fig. 6. Uncertainties to these values are discussed in next sections. The resulting wavelength dependent efficiency is shown in Fig. 7 where the fitting was done adjusting the piecewise function to the

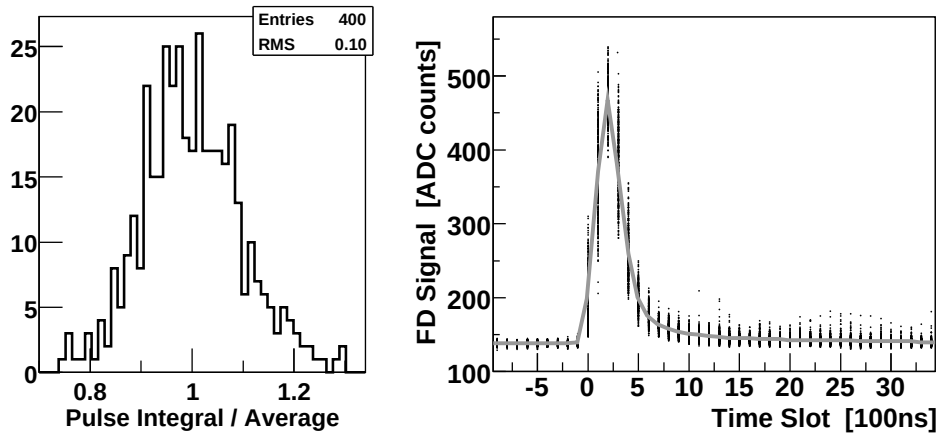

Figure 5: FD single pixel response to drum pulses. The signal of pixel number 220 of telescope 4 with drum at 355 nm is shown. Left: Distribution of pulse integrals related to the average integral. Right: Pulses as registered by the FD. Dots are the values for 400 individual pulses. The grey solid line is the average

five measured points R_i^{rel}. The piecewise response in its original form is also shown in the figure for comparison purposes. The fit has been corrected for notch-filter width effects, as described in next section.

5.1. Notch Filter Width Effects and fitting procedure

In section 4.3 we described how the drum centroids for five wavelengths were measured and corrected for the lab-PMT quantum efficiency to get the relative drum intensities. In that process the change in the QE was taken into account by considering the distribution of photons for each notch-filter. Then, in section 5, we described how the FD responses to those intensities were measured for one FD telescope. In this last process the notch-filter width effect was not taken into account. Because the overall FD response is not flat in the ∼15 nm FWHM range of each filter, this uncorrected result is biased toward the region of the filter corresponding to higher FD response.

To correct for this effect we follow a similar procedure as in section 4.3. The process at the telescope is:

$$\frac{\int \Phi_i(\lambda)\ FD(\lambda)\ d\lambda}{\int \Phi_i(\lambda)\ d\lambda} = R_i^{rel} \tag{2}$$

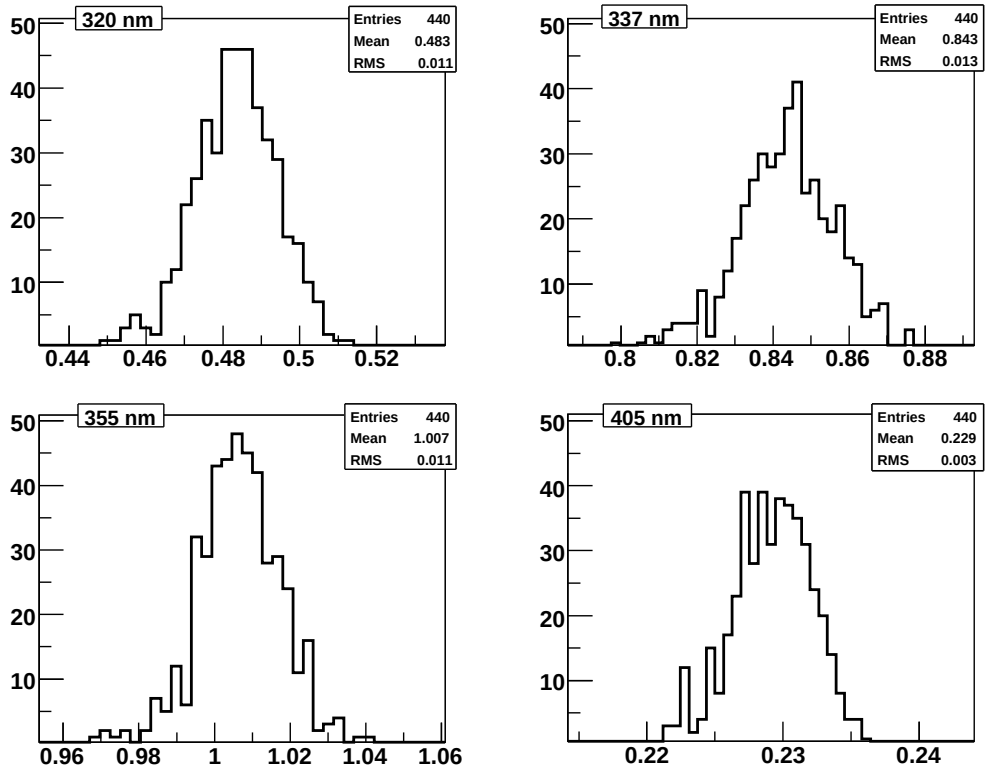

Figure 6: Distribution of relative FD response for each notch-filter. The response relative to 380 mn of all pixels in one telescope is shown

where $FD(\lambda)$ is the FD relative response as a function of wavelength. Again, we are not including wavelength independent constants as this is a relative measurement procedure. Note that if the notch-filter transmission, $f_i(\lambda)$, were delta functions at λ_i, we would have $FD(\lambda_i) = R_i^{rel}$. To solve the integral of equation 2 and find the unknown function $FD(\lambda)$ we made the assumption that the FD response is a piecewise-like function, as described in section 2. This choice is required because the five measurements in the wavelength range of the FD response are not sufficient to fully characterise a generic function. Then, it is reasonable to adjust the original piecewise function, $PW(\lambda)$, to what was measured. This assumption also implies that we have taken the FD response as null beyond the wavelength of the FD

Wavelength	R_i^{rel}	
(nm)	Mean	Corrected
320	0.483	0.409
337	0.843	0.832
355	1.007	0.998
380	1.000	1.044
405	0.229	0.243

Table 1: Average relative FD response measured for each notch-filter. Values are taken from the distributions of Fig. 6. The column on the right have the values after the correction for notch-filter width effects as described in section 5.1

system. Particularly, we take $FD(280\ nm) = FD(425\ nm) = 0$, which have been verified by measuring the UV-filter transmission in our laboratory.

The procedure of adjusting the fitting function to the measured points was as follows. For each notch-filter we take $FD(\lambda) = h_i Fit(\lambda)$, where $Fit(\lambda)$ is the fitting function and h_i a parameter for filter i. As a first guess the piecewise function is taken so, $Fit(\lambda) = PW(\lambda)$. Equation 2 is evaluated and the parameter h_i found to match the value R_i^{rel}. Once all five h_i are found, a new fit is done by interpolating the points $h_i Fit(\lambda_i)$ with a piecewise-like function, where now i runs for seven points, including the null extremes. Between these points, the curve is adjusted by a linear interpolation of the adjustments at the surrounding points. Finally, this last fit is taken as a new $Fit(\lambda)$ function and the process starts again until all five values h_i are the identity.

The final result of the iteration procedure, $Fit(\lambda)$, is the $FD(\lambda)$ that fulfils the integral in equation 2 for all five measured points. This curve is shown in Fig. 7, normalised to the value at 380 nm. In the same figure we also show the original piecewise function. A decrease in the spectral response compared to the piecewise response is observed at shorter wavelengths, the largest difference of $\approx$ -28% comes at 320 nm. The corrected R_i^{rel} values are shown in Table 1.

5.2. Uncertainties

Contributions to the uncertainty include those from measurements in the laboratory of the drum intensity, and from measurements at the telescope of the FD response. The overall result reported here is a relative measurement, and consequently many factors cancel particularly systematics related

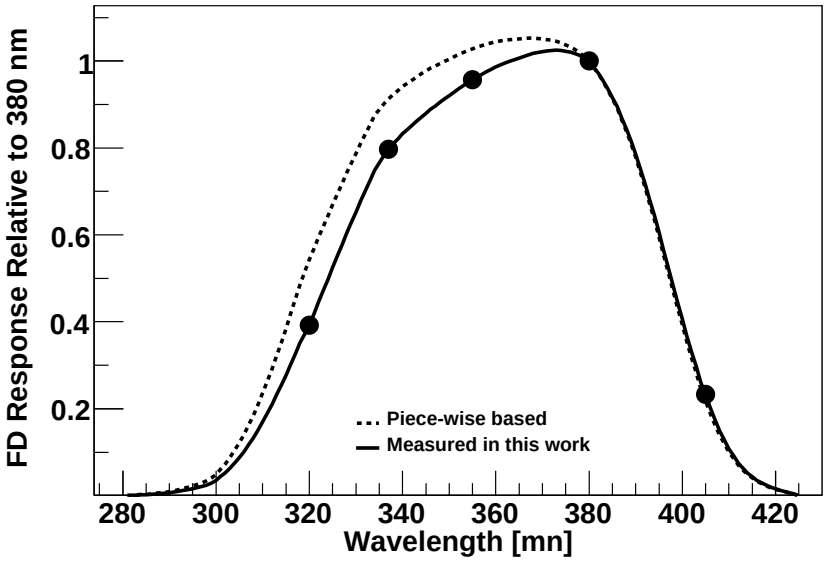

Figure 7: The measured Fluorescence Detector wavelength response compared with a curve generated in a piecewise fashion from manufacturer's data for each FD component. The corrected measurements at the 5 wavelengths are shown; the solid curve is constrained to pass through those points

to laboratory setup.

The determination of drum intensity at each wavelength includes measurements in the laboratory of the centroid of the lab-PMT response to pulsed drum illumination, and the relative QE of the lab-PMT. The uncertainty in the lab-PMT drum response centroid, C_i in equation 1, is estimated to be 1 channel in the ADC converter plus the statistical uncertainty on the mean of the 1000 xenon pulse distribution. The 1 channel uncertainty is a systematic effect, related to repeatability, and has more relevance for wavelengths where the drum brightness is low. The second column in Table 2 indicates the uncertainties in C_i.

Uncertainties related to measurement of the relative QE of the lab-PMT include those from lab-PMT response, photodiode current during monochromator scans, the calibration of the photodiode at each wavelength, and systematics in the laboratory setup. The uncertainty in the monochromator

Wavelength (nm)	C_i (%)	Φ_i (%)	R_i^{rel} (%) Statistical	Systematic	Total
320	0.6	2.6	2.2	4.1	4.7
337	1.0	2.7	1.5	4.2	4.5
355	2.0	3.2	1.1	4.5	4.6
380	2.0	3.2	n/a	0.0	0.0
405	0.3	2.5	1.3	4.1	4.3

Table 2: Sources of uncertainties and their values for this work (see section 5.2).

wavelength has been measured with a N2 laser light source to be less than ∼0.25 nm, and no contribution to the overall uncertainty has been included for this effect.

For the PMT QE scans, currents from the photodiode and the lab-PMT were measured with electronics based on an integration chip with linearity of 0.005% [13]. Effects of connectors and cabling between the detectors and the integration chips are expected to dominate any nonlinearities. While these effects are expected to be small, we assign an overall uncertainty of 2% to current measurements, based on our experience measuring absolute currents using similar configurations. For this relative measurement, the experimental configuration remained unchanged during measurements at different wavelengths, allowing some readout systematics to cancel in the final ratios. The uncertainties in the absolute response of the photodiode, as calibrated by NIST, are documented as k=2 expanded uncertainties [12]. Assuming normal distributions for the contributing factors, these can be interpreted as 1-sigma uncertainties varying in the range from 0.55 to 0.95% for wavelengths between 300 and 400 nm, and 0.4% or less for those between 405 and 450 nm. Monochromator output beam uniformity has been measured in the PMT-photodiode region to be better than 0.5% across a 10 cm region perpendicular to the beam. No contribution to the overall uncertainty has been included for beam non-uniformity. The stability of the system, including the lab-PMT response, was tested by performing measurements multiple times to find that repeatability is well within 1%. As a result of these effects we consider an overall uncertainty of 2.5% for the relative QE of the lab-PMT. Combination of the uncertainties of C_i and QE give the uncertainty in the drum brightness, Φ_i, as listed in Table 2.

The camera–averaged response of pixels to each of the five wavelengths are described in section 5. To evaluate the uncertainties in these responses we consider the systematics coming from drum fluxes, Φ_i as discussed above, and the widths of the distributions of responses for the 440 pixels in the camera, as taken from the distributions of Figure 6 and shown in the fourth column of Table 2. For a given pixel j, $R_{ij}^{rel} = R_{ij}/R_{4j}$, four quantities have to be considered: two integrals, I_{ij} and I_{4j}, and two drum fluxes, Φ_i and Φ_4, as defined in previous sections. Uncertainties in the integrals are purely statistical and have been evaluated to be <0.5 %. The combination of these four values gives the total uncertainty shown in the fifth column of Table 2. Values at different wavelengths are independent and are added in quadrature, except at 380 nm where systematic uncertainties are null by definition. The last column in Table 2 shows the combined uncertainty for the two sources.

Finally, we consider uncertainties resulting from the fitting procedure incorporating the effects of the notch-filter widths, as described in section 5.1. The shape of the piecewise calibration curve, used as the initial fitting function, is dominated near 300 nm by the fall-off of FD PMT quantum efficiency at shorter wavelengths, and by decreasing transmission of the UV filter through the FD aperture above 400 nm. We have tried several shapes for this initial function and found that any reasonable choice incorporating these two features leads to near-identical results. No related uncertainty is included.

When applying the notch-filter width correction we use the relative transmission of the 5 notch filters, measured as described in section 4.1. Associated uncertainties are 0.5% at each wavelength in the scans. Good correlation with the manufacturer's scan available for one filter supports this value of the uncertainty. For an independent evaluation of the systematics related to filter shape, we took the wavelength with the largest filter-width effect, 320 nm, and changed the filter shape to an extreme-case scenario of a step function. We included a maximum spread in intensity between two wavelengths by assuming extremes of the photodiode uncertainties at the respective wavelengths. We then repeated the notch filter correction calculation. The corrected value of R_1^{rel} given in Table 1 changed by -0.5 %, supporting the assesment above.

Based on the discussions above, we assign an overall total uncertainty of 5 % to the measurements reported here. The main contributions come from the uncertainties on the relative QE of the lab-PMT and the measured

relative drum fluxes at each wavelength.

6. Conclusions

The method for measuring the relative wavelength-dependence response of the Pierre Auger fluorescence detector has been tested in one telescope. Within uncertainties we can say that a multi-wavelength calibration for each PMT in a given camera is not necessary as the dispersion around the average is of the order of few percent.

This result indicates lower FD efficiency at shorter wavelengths when compared to a curve constructed in a piecewise manner from manufacturer efficiency specifications for the individual elements of the system. The piecewise curve was adjusted to the measured values and the result is currently used in the Auger event reconstruction software.

References

[1] J. Abraham [Pierre Auger Collaboration], NIM A 523 (2004) 50-95.

[2] M. Roth [Pierre Auger Collaboration], Proceeding 30^{th} ICRC, Merida (2007).

[3] J. Abraham [Pierre Auger Collaboration], Physical Review Letters 101 (2008), 061101.

[4] V. Verzi [Pierre Auger Collaboration], Nucl. Phys. B (Proc. Suppl.) 165 (2007) 37.

[5] R. Knapik [Pierre Auger Collaboration], Proceeding 30^{th} ICRC, Merida (2007).

[6] C. Aramo [Pierre Auger Collaboration], Proceeding 29^{th} ICRC, Pune (2005), 8, 101.

[7] J. T. Brack, *et al.*, Astropart. Phys. 20 (2004) 653.

[8] P. Bauleo [Pierre Auger Collaboration], Proceeding 29^{th} ICRC, Pune (2005), 8, 5-8.

[9] J. A. J. Matthews [Pierre Auger Collaboration], Proceeding SPIE Astronomical Telescopes and Instrumentation, Waikoloa , Hawaii (2003), 4858, 121-130.

[10] G. Matthiae [Pierre Auger Collaboration], Proceeding 27^{th} ICRC, Hamburg (2001).

[11] M. Nagano, *et al.*, Astropart.Phys. 20 (2003) 293.

[12] T.C. Larson, S.S. Bruce, and A.C. Parr, "Spectroradiometric Detector Measurements", National Institute of Standards and Technology, Calibration Program, Gaithersburg, MD 20899-2330, Special Publication 250-41, 1998.

[13] Burr-Brown Corporation, chip ivc102; http://www.burr-brown.com/